Applied Biochemistry and Biotechnology
https://doi.org/10.1007/s12010-019-03078-y

Kinetic and Thermodynamic Investigation of Human Serum Albumin Interaction with Anticancer Glycine Derivative of Platinum Complex by Using Spectroscopic Methods and Molecular Docking

Afrooz Shiekhzadeh[1] · Nasrin Sohrabi[1] · Mahboube Eslami Moghadam[2] · Mohsen Oftadeh[1]

Received: 8 February 2019 / Accepted: 5 July 2019/Published online: 07 August 2019

Abstract

In this paper, a new anticancer Pt (II) complex, *cis*-[Pt $(NH_3)_2$(tertpentylgly)]NO_3, was synthesized with glycine-derivative ligand and characterized. Cytotoxicity of this water-soluble Pt complex was studied against human cancer breast cell line of MCF-7. The interaction of human serum albumin (HSA) with Pt complex was studied by using UV-Vis, fluorescence spectroscopy methods, and molecular docking at 27 and 37 °C in the physiological situation ($I = 10$ mM, pH = 7.4). The negative ΔH_b^0 and positive ΔS_b^0 indicated that electrostatic force may be a major mode in the binding between Pt complex and HSA. Binding constant values were obtained through UV-Vis and fluorescence spectroscopy that reveal strong interaction. The negative Gibbs free energy that was obtained by using the UV-Vis method offers spontaneous interaction. Fluorescence quenching the intensity of HSA by adding Pt complex confirms the static mode of interaction is effective for this binding process. Hill coefficients, n_H, Hill constant, k_H, complex aggregation number around HSA, <*J*>, number of binding sites, g, HSA melting temperature, T_m, and Stern-Volmer constant, k_{SV}, were also obtained. The kinetics of the interaction was studied, which showed a second-order kinetic. The results of molecular docking demonstrate the position of binding of Pt complex on HSA is the site I in the subdomain IIA.

Keywords Human serum albumin · Fluorescence quenching · Pt complex · Tertpentyl glycine · Molecular docking

✉ Nasrin Sohrabi
sohrabnas@pnu.ac.ir; nsohrabi48@jmail.com

✉ Mahboube Eslami Moghadam
eslami_moghadam@ccerci.ac.ir; eslami_moghadam@yahoo.com

Extended author information available on the last page of the article

Abbreviations

HSA	Human serum albumin
PDB	Protein Data Bank
Tertpentylgly	1,1-Dimethyl propyl glycine

Introduction

Human serum albumin (HSA), as the most plentiful carrier protein, has many significant physiological activities. Among its functions, metallodrugs get free in targeting organs via binding with albumin protein. Hence, HSA cannot protect metallodrugs after binding against oxidation, aquation, distribution, and the stability of drug changes [1].

Metal drugs are bound and unbound to HSA in plasma circulation. The unbound drugs spread in the blood, and they are metabolized distributed intracellularly via particular forwarding systems [2]. Also, free drug molecules can interact effective with hurt targets [3]. In most case, the unbound drug concentration in plasma should be determined and controlled [3].

Therefore, the investigation of reversible HSA-complex interactions is necessary for following the pharmacokinetics and dynamics effects of drugs. Also, in more cases, the solubility of hydrophobic drugs can be improved by interaction with serum albumin [4]. Hence, protein-drug binding study provides valuable data for understanding the effect of drug in vivo processes. Platinum (II) complexes as anticancer drugs, for example, cisplatin, are known and used with high chemotherapeutic affect for treatment of several types of cancer, some tumors, and ovarian and head and neck carcinomas [5].

Binding of Pt complexes on serum albumin is necessary for their biotransformation in biological fluids, but because of binding of platinum center with protein contains sulfur atoms, serious side effects cause. Hence, more Pt complexes are designing, and new agents are being synthesized with lower toxicity [6]. In this case, redox activity of metal center and selectivity bind to bimolecular target should be attended. Some methods and several spectroscopic techniques such as fluorescence and absorption employ conformational properties of the protein and drug-protein [7, 8]. In recent years, various investigations have been done on the interaction of anticancer platinum and palladium derivatives with human serum albumin [9–20].

In the present research, a platinum (II) complex, *cis*-[Pt $(NH_3)_2$(tertpentylgly)]NO_3, was synthesized and characterized (Scheme 1). The HSA interaction with this water-soluble Pt complex was studied by using electronic absorption and fluorescence spectroscopies and also

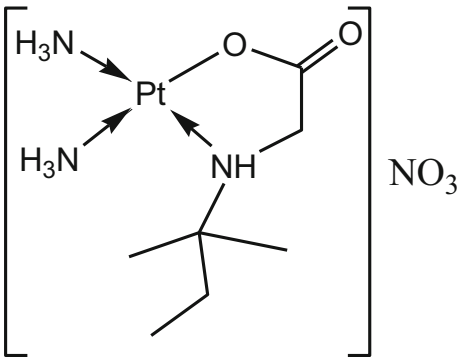

Scheme 1 The proposed structure of *cis*-[Pt $(NH_3)_2$(tertpentylgly)]NO_3 complex

modeled by molecular docking. Based on these studies, the important information about thermodynamic parameters and the modes and mechanism and also the location of the connection were determined. Then, the enthalpy (ΔH_b°), entropy (ΔS_b°), and Gibbs free energy (ΔG_b°) changes, melting point of HSA in the absence and presence of complex, T_m, the aggregation number complex around HSA, $\langle J \rangle$, computed and estimated the number of binding sites, g, binding constants, K_b, Hill coefficient, n_H, Stern-Volmer coefficient, K_b, quenching constant, k_q, and the mechanism of quenching. In addition, cytotoxicity of this new complex has been tested against human breast cancer cell line of MCF-7. These results would be expected to help realize the binding mode of this Pt (II) complex to protein.

Experimental

Materials and Instrumentation

Silver nitrate, potassium iodide, tertpentyl amine, ammonia, sodium bicarbonate, and potassium tetrachloroplatinate were purchased from Merck (Germany). Solvents such as acetone, ethanol, and anhydrous diethyl ether were obtained from Merck Co. (Germany). Human serum albumin (HSA, purity > 99.0%) was bought from Sigma-Aldrich Co. (USA) and stored at 4.0 °C. The stock solution of the Pt (II) complex (2 mM) was prepared with Tris-HCl buffer containing NaCl (10 mM, pH 7.4). The HSA stock solution was diluted to 0.03 mM with the same buffer.

Infrared spectra were measured on a FTIR 8400 Shimadzu spectrometer from 4000 to 400 cm^{-1}using KBr pellets. ^1H NMR (300 MHz) spectrum was collected on Bruker BRX-250 Avance spectrometer with reference as DMSO − d_6 solvent. The melting point of complex was determined on a Buchi (Flawil, Switzerland) melting point B-545. Conductivity measurement was carried out by a TetraCon 325 electrode connected to a Terminal 740 (WTW, Germany) with a cell constant of 0.951 using conductivity water as the solvent. Elemental analysis (C, H, and N) of complex that was performed by a CHN has been analyzed by Elementar Analysensysteme GmbH-Vario EL III.

All fluorescence spectra were carried out on a Scinco FS-2 fluorescence spectrophotometer in 200–700 nm. UV spectra of free HSA and HSA in the presence of various concentrations of Pt (II) complex were measured using the PerkinElmer Precisely Lambda 25 Spectrophotometer in 200–700 nm.

Synthesis of *cis*-[Pt $(NH_3)_2$(tertpentylgly)]NO_3

Tertpentyl glycine was synthesized the way it was previously published and used for synthesis of complex [21]. Also *cis* − $[Pt(NH_3)_2I_2]$ was prepared according to the method described previously [22]. 0.183 mmol (0.088 g) *cis* − $[Pt(NH_3)_2I_2]$ and 0.367 mmol (0.062 g) $AgNO_3$ were suspended in 18 mL double-distilled water under continuous stirring condition for 24 h at room temperature and then refluxed at 50 °C for 30 min under darkness. Then, gray AgI precipitate was removed by centrifugation. After that, the solution of 0.183 mmol (0.033 g) tertpentyl glycine hydrochloride and 10 mL solution of 0.366 mmol (0.03 g) $NaHCO_3$ in water were added to above centrifuged solution and stirred at 40 °C for 4 h. The solution was evaporated to 1 mL until the brown precipitate appeared. The obtained product was decanted and washed by chilly acetone and dried in a desiccator. Scheme 2 shows the formation of complex.

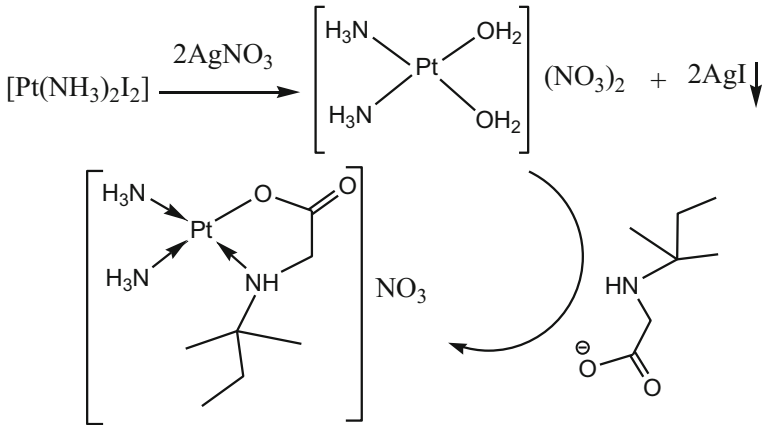

Scheme 2 General procedure of complex formation

cis-[Pt $(NH_3)_2$(tertpentylgly)]NO_3 (435.08 g/mol): the yield is 69%; mp (160–165 °C); analytical calculated for $C_7H_{20}N_3O_2Pt$ compound is C, 19.30, H, 4.59, N, 9.65%, analytical found: C, 18.93, H, 4.20, N, 9.37%; UV: λ_{max} nm (ε_M): 201 (28.8); molar conductance, ΛM (10^{-4} M, H_2O) = 120 Ω^{-1} cm^2 mol^{-1}; FTIR (cm^{-1}, KBr disk): 3432 (s, N-H), 3283 (s, C-H), 1627 (s, C=O), 1361 (s, $(NO_3)^-$); ^{1}H NMR (300 MHz, DMSO-d_6, δ in ppm, J in Hz): 1.12 (*t*, J = 9 Hz 3H), 1.21 (m, 2H), 1.62 (s, 6H), 2.07 (d, 2H), 4.4 (m, 7H $_{NH}$).

Cell Culture and Cell Proliferation Assay

Human breast cancer cell line of MCF-7 was purchased from the National Cell Bank of Iran (NCBI), Pasteur Institute of Iran. The cells were grown on the DMEM medium (Sigma) supplemented with L-glutamine (2 mM), streptomycin, penicillin (5 $\frac{\mu g}{mL}$), and 10% heat-inactivated fetal calf serum at 37 °C under 50%: 95% CO_2; air atmosphere. The cytotoxicity activity of new synthesized complex was studied by MTT assay. The harvested cancer cells of MCF-7 were seeded into a 96-well plate ($1 \times 10^4 \frac{cell}{mL}$) and incubated with various concentrations of sterilized *cis*-[Pt $(NH_3)_2$(tertpentylgly)]NO_3 (0–800 μM) for 24 h. IC_{50} value determination was done according to the published method in Ref [23].

Evaluation of Thermodynamic Parameters

Absorption recording is an easy and suitable method to investigate the complex-HSA formation [24, 25]. A working solution of HSA and Pt complex was diluted to 15 μM and 0.8 mM, respectively. Then, the injection of complex to HSA solution was continued up to the point that no further changes in the absorption were shown. The spectra were recorded from 200 to 700 nm in a quartz cuvette (total cuvette volume was 1000 μL) at 27 and 37 °C.

Fluorescence Studies

The fluorescence intensity of protein may be quenched by adding of metal complex, when complex interacts with HSA. In this study, the fluorescence intensity was monitored by excitation wavelength at 280 nm and emission wavelength limited area of 200–700 nm. In

each measurement, HSA-Pt complex was allowed to incubate for 5 min after the addition of each complex. Both excitation and emission band cross were kept at 5 nm [26].

Electrochemical Measurement

Cyclic voltammetry (CV) study was done by Potentiostat/Galvanostat Autolab. Glassy carbon, platinum wire, and the working auxiliary and the reference electrode were Ag/AgCl/3 M KCl, respectively. This experiment was carried out at room temperature and 100 mV s^{-1} scan rate. Concentration of Pt complex was 0.1 mM in Tris buffer with 10 μM and without HSA.

Docking

Docking study can determine the active binding site for Pt complex on HSA. The 3D structure of the *cis*-[Pt $(NH_3)_2$(tertpentylgly)]NO_3 was generated using HyperChem software, and its geometry was optimized using Gaussian 03 software by the *DFT-B3LYP* method at the level of 6–31 g* [27]. The crystal structure of HSA (PDB ID: 5ORI) was selected from the Protein Data Bank in pH = 7.4 (http://www.rcsb.org/pdb). Here, the *R* value and resolution of this file were 0.218 and 0.25 Å, respectively. Water molecules of the 5ORI pdb file were removed, and missing hydrogen atoms and Gasteiger charges were added. Also, the flexible-ligand docking was done via the AutoDock 4.2 molecular docking program (http://autodock.scripps.edu) and using experimental free energy function and the Lamarckian genetic algorithm [27].

Results and Discussion

In Vitro Cytotoxicity Studies

Anticancer activity of *cis*-[Pt $(NH_3)_2$(tertpentylgly)]NO_3 against human breast cell line of MCF-7 was done. MCF-7 cells as experimental metastasis model were incubated in the absence and presence of various concentrations of Pt complex (0 − 800 μM) at 37 °C for 24 h incubation times [28]. Figure 1 and cytotoxicity data show that the human breast cell line

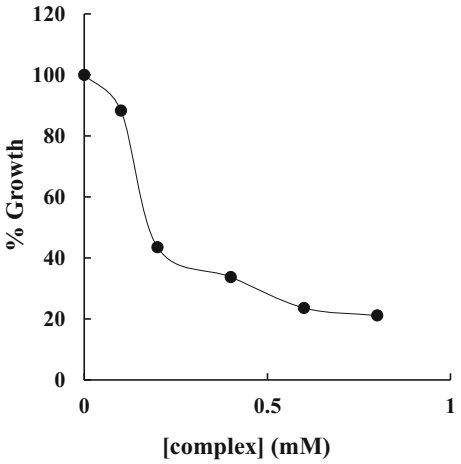

Fig. 1 Growth suppression activity of Pt complex on MCF-7 cell lines incubated with varying concentrations of the complex for 24 h using MTT assay

is reduced by increasing the concentration of Pt complex. IC_{50}value was calculated 175 μM. In this study, cisplatin was used as a common chemotherapy drug for positive control with IC_{50} equal to 80 μM, which is lower than IC_{50} value of synthesized Pt complex. According to data, it is obvious that *cis*-[Pt $(NH_3)_2$(tertpentylgly)]NO_3 with tertpentyl hydrocarbon chain shows anticancer activity against human breast cancer cell line of MCF7 not as good as cisplatin, but the presence of bidentate N-O ligand in the structure of synthesized compound properly leads to less side effect of clinical drug with the same or lower IC_{50} value. Also, similar compounds aromatic N,N dentate have been reported with IC_{50} about 40~70 μm against breast cell line of MDA-MB231 [21]. Then, it can be concluded that the presence of aliphatic N,N group or amine groups can reduce anticancer activity, whereas the presence of aromatic N,N group increased the cytotoxicity activity of Pt (II) complexes.

HSA Binding Data

The absorption spectra of HSA before and after the addition of Pt complex are shown in Fig. 2. This figure demonstrates that the absorption values are reduced by increasing the concentration of Pt complex because due to the interaction between protein and complex, the protein-complex is formed with certain new formal structures [29].

The values of the concentration of complex in the midpoint of transition of natural HSA to the binding state, $L_{\frac{1}{2}}$, were decreased by increasing the temperature. It is due to the descending stability of the HSA-Pt complex. The values of $L_{\frac{1}{2}}$ show that complex could be bind to HSA in low concentrations. Cytotoxicity results also show this synthesized Pt (II) complex can probably be used as anticancer agents with low dosage and few side effects [30]. This diagram is shown in Fig. 3.

The value of binding constant, K_b, was obtained by using Eq. 1.

$$\frac{1}{A-A_0}=\frac{1}{A_\infty-A_0}+\frac{1}{K_b[A_\infty-A_0]}\cdot\frac{1}{[\text{complex}]} \tag{1}$$

where $A_0$is the primal absorption of HSA at 278 nm in the absence of metal complex. $A_\infty$is the terminal absorption of HSA, and A is the recorded absorption at various concentrations of the complex. The binding constant (K_b) can be calculated through the intercept to the gradient of the linear curve of $\frac{1}{A-A_0}$ vs. $\frac{1}{[\text{complex}]}$ [31]. This diagram is shown in Fig. 4.

Binding free energy, ΔG_b°, was obtained at 298 K using Eq. 2 [32].

$$\Delta G_b^\circ=-RT\ln K_b \tag{2}$$

Also, the thermodynamic parameters can be obtained by using the equation of van′t Hoff as follows:

$$\ln\frac{K_2}{K_1}=-\frac{\Delta H}{R}\left(\frac{1}{T_2}-\frac{1}{T_1}\right) \tag{3}$$

$$\Delta G_b^\circ=\Delta H_b^\circ-T\Delta S_b^\circ=-RT\ln K_b \tag{4}$$

Here, K and $T$are considered at two temperatures. The thermodynamic parameters of a binding reaction between Pt complex and HSA such as enthalpy change (ΔH°), entropy change (ΔS°),

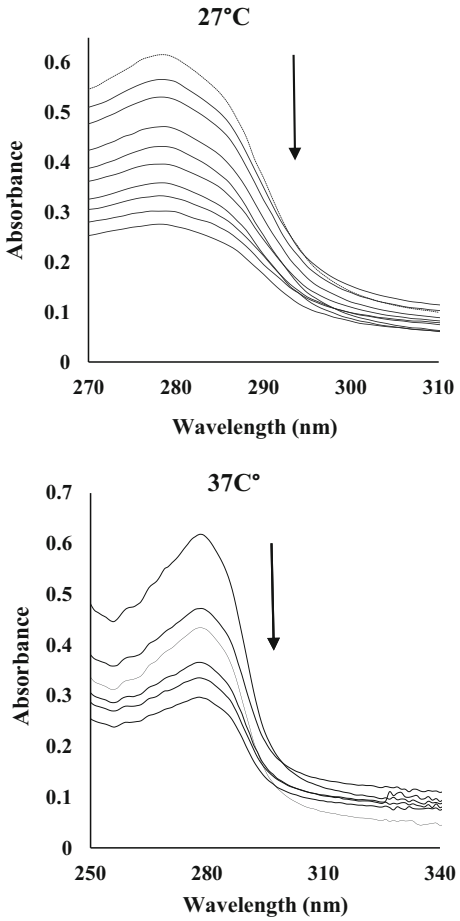

Fig. 2 Absorption spectra of HSA (15 μM) in the absence and the presence of *cis*-[Pt $(NH_3)_2$(tertpentylgly)]NO_3 in Tris-HCl buffer-10 mM NaCl (pH = 7.4) at 27 and 37 °C

and free energy change ($\Delta G°$) are the principal evidence which can be used to determine the binding type (Eq. 4). The negative amounts of ΔG_b° indicate complex-protein binding procedure is spontaneous. As usual, $\Delta H° > 0$ and $\Delta S° > 0$ imply a hydrophobic interaction; $\Delta H° < 0$ and $\Delta S° < 0$ display the van der Waals force or hydrogen bond formation, and $\Delta H° > 0$ and $\Delta S° > 0$ offer an electrostatic force [4].

The negative ΔH_b° and positive ΔS_b° amounts offer electrostatic force that plays the main role in the complex-HSA interaction [33]. These parameters are listed in Table 1.

Binding Isotherm

The binding isotherm of protein with complex can be easily obtained by carrying out titration in several different concentrations of Pt complex at 27 and 37 °C. These plots are shown in Fig. 5. Comparing these binding isotherms with binding isotherm of oxygen to hemoglobin, it is obvious that the binding of Pt complex to HSA has one binding set [34].

Structural changes upon ligand binding first revealed by X-ray crystallography for hemoglobin have now been for several other proteins. These findings emphasize the general nature of structure and of ligand control or allosteric effect. The conformation suitability of HSA

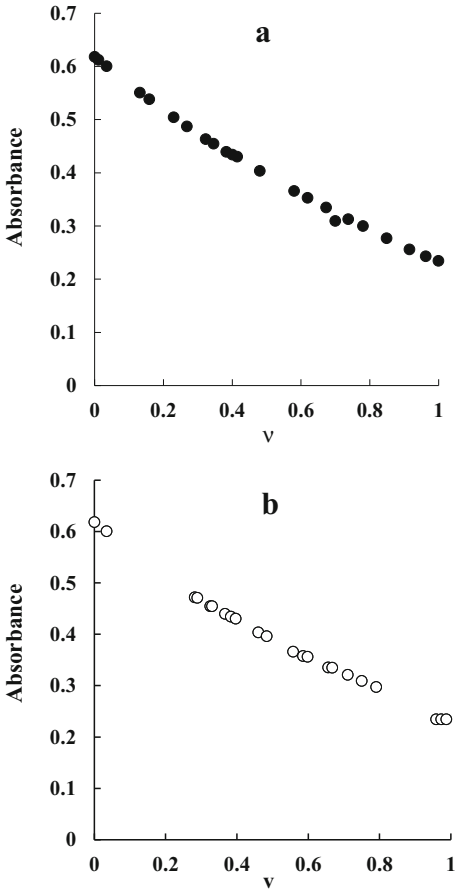

Fig. 3 HSA absorbance at 278 nm vs. ν ($\nu = [\text{complex}]_t/[\text{HSA}]_t$) at 27 (**a**) and 37 °C (**b**)

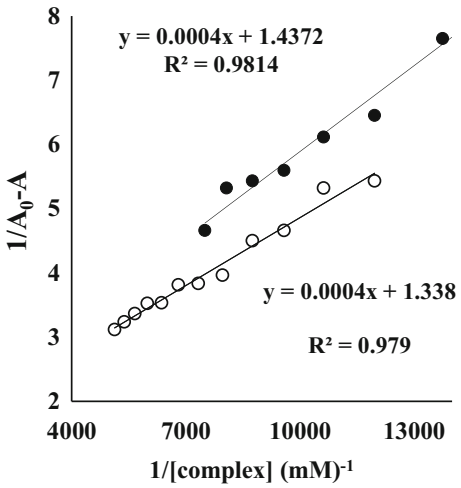

Fig. 4 The linear plot of the reciprocal of ΔA vs. the reciprocal of *cis*-[Pt $(NH_3)_2$(tertpentylgly)]NO_3 at 27 °C (●) and 37 °C (○)

Table 1 Thermodynamic parameters and $L_{1/2}$ value of HSA binding with platinum (II) complex

Complex	Temperature (°C)	$L_{1/2}$ (mM)	$\Delta G_b°$ (kJ mol^{-1})	$\Delta H_b°$ (kJ mol^{-1})	$\Delta S_b°$ (J mol^{-1} K^{1})
cis-[Pt $(NH_3)_2$(tertpentylgly)]NO_3	27	0.12	−20.4	−5.5	+49.7

involves more than the immediate affinity of the binding site(s). This is related to the observed ligand-dependent allosteric conformational transition(s) [35].

Due to these points, the above binding represents one binding set with allosteric effect. This kind of binding causes positive cooperativity. The binding capacity diagram consists of a series of sequential maxima, which should be equal to the number of binding sets. The positions of the maxima determine the binding sites in each binding set [34].

$$\theta = \frac{n_H \nu (g - \nu)}{gRT} \tag{5}$$

$$\frac{RT\theta}{\nu} = n_H - \frac{n_H \nu}{g} \tag{6}$$

Equations 5 and 6 offer that the plot of $\frac{RT\theta}{\nu}$ vs. ν for a system should be linear (Fig. 6) with g identical and dependent binding sites [34].

Scatchard Plot on Interaction of HSA with Complex

The Scatchard plots ($\frac{\nu}{[\text{complex}]_f}$ vs. ν) are shown in Fig. 7 for the interaction of HSA with complex at both temperatures of 27 and 37 °C. ν is the ratio of $\frac{[\text{complex}]}{[\text{HSA}]}$ in transition region with cooperative binding [36].

The Scatchard equation is as follows [30]:

$$\frac{\nu}{[\text{complex}]} = K^0(g - \nu) \tag{7}$$

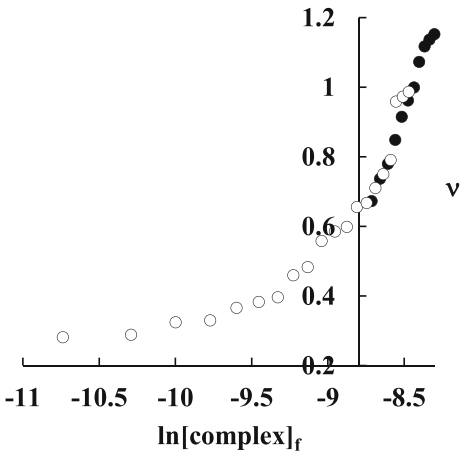

Fig. 5 The binding isotherm of HSA with complex at 27 °C (●) and 37 °C (○)

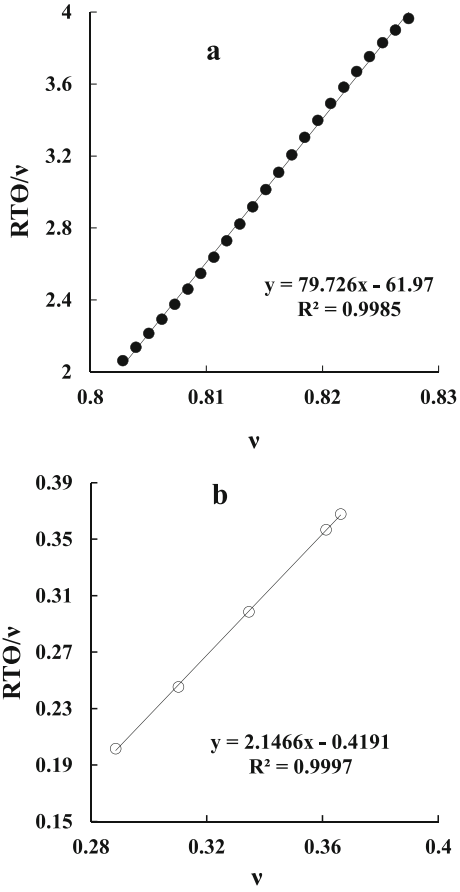

Fig. 6 The plot of $\frac{RT\theta}{\nu}$ vs. ν for the interaction of complex with HSA at 27 (**a**) and 37 °C (**b**)

The number of binding sites (g) of Pt complex on HSA can be obtained. Also, Hill plot of the interaction of HSA with complex has been shown in Eq. 8 [30] (Fig. 8).

$$\ln\left(\frac{\nu}{g-\nu}\right) = \ln K_H + n_H \ln[\text{complex}]_f \tag{8}$$

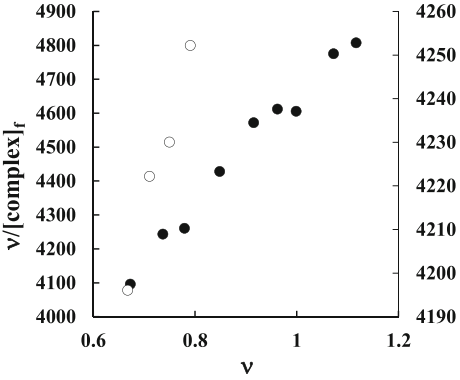

Fig. 7 Scatchard plot for HSA binding with complex at temperature of 27 °C (●) and 37 °C (○)

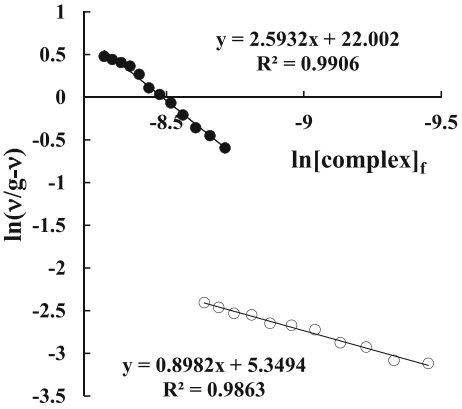

Fig. 8 Hill plot of HSA binding with complex at temperature of 27 °C (●) and 37 °C (○)

By plotting the $\ln\left(\frac{\nu}{g-\nu}\right)$ vs. the ln[complex]$_f$, Hill plot is obtained, and several parameters of the cooperative binding interaction can be determined, as shown in Fig. 8. The obtained Hill coefficient is more than one, which means the type of cooperativity is positive [37]. Results are summarized in Table 2.

The molar intrinsic site-site interaction Gibbs free energy change of *cis*-[Pt $(NH_3)_2$(tertpentylgly)]NO_3-HSA is usually calculated by the following relationship (Eq. 9) [38] as shown in Fig. 9, where [complex]$_f$ in Eq. 9 is free *cis*-[Pt $(NH_3)_2$(tertpentylgly)]NO_3 concentration.

$$\Delta G_b^0 = -RTn_H \ln K_H + RT\,(1-n_H)\ln[\text{complex}]_f \tag{9}$$

Eventually, we can conclude that all of the binding processes show positive cooperativity in the binding set [33].

Thermal Stability of HSA

This experiment was carried out by monitoring the UV-Vis absorption of HSA (7.5 μM) in Tris buffer (pH 7.4) at 278 nm in the absence and presence of the complex (0.8 mM) and heated from 25 to 75 °C with 1 °C min^{-1}. It is shown in Fig. 10. Data show the stability of HSA was increased in the presence of complex [39]. T_m values (the melting temperature) were defined 46 and 53 °C in the absence and presence of Pt complex ($\Delta T_m = 7\,^\circ\text{C} \pm 1\,^\circ\text{C}$).

T_m was taken for the free HSA without ligand and in a molar ratio of Pt complex to HSA upper than $L_{1/2}$.The results of such studies for Pt complex-HSA complex are shown in Fig. 11. By using Igor software and determining $\frac{\partial \Delta\varepsilon}{\partial \Delta T}$, T_m is obtained and listed in Table 3. Data show the increasing of T_m by adding the complex concentration and the denaturation process between two states, that is, from the native state (N) to a denatured state (D).

Table 2 Hill parameter and binding constant of HSA interaction with complex

Complex	Temperature (°C)	g	K_b (M^{-1})	K_H(M^{-1})	n_H
cis-[Pt $(NH_3)_2$(tertpentylgly)]NO_3	27	1.9	3.6×10^3	391.9	22.0
	37	9.0	3.3×10^3	7.9	5.35

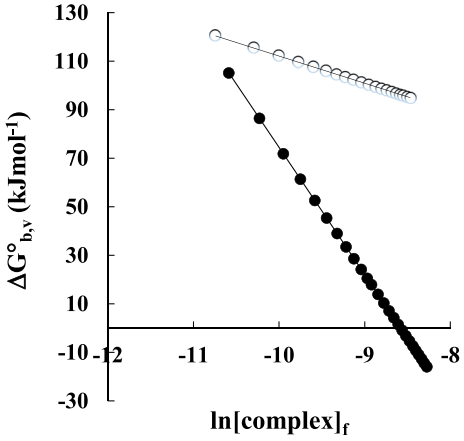

Fig. 9 The variation of $\Delta G^0_{b,v}$ vs. ln[complex]$_f$ for HSA interaction with complex at 27 °C (●) and 37 °C (○)

The protein stability is usually stated by the Gibbs free energy values since ΔG_D is the work required for disruption of the native protein structure. Hence, by using Gibbs-Helmholtz (Eq. 10), the difference in Gibbs energy can be expressed at a given temperature.

$$\Delta G_D(T) = \Delta H_m\left(1-\frac{T}{T_m}\right)-\Delta C_p\left[(T_m-T)+T\ln\frac{T}{T_m}\right] \tag{10}$$

Also, other parameter as the equation constant (k) can be obtained based on spectroscopic techniques, in transition region and it is deduced from Eq. 11 [40].

$$k=\frac{[D]}{[N]}=\frac{(A_N-A_0)}{(A_0-A_D)} \tag{11}$$

where A_N, A_D, and A_0 are the absorption of native, denatured, and observed area at any temperature. For at least errors, all the experimental data points were obtained and fitted in the equation as follows:

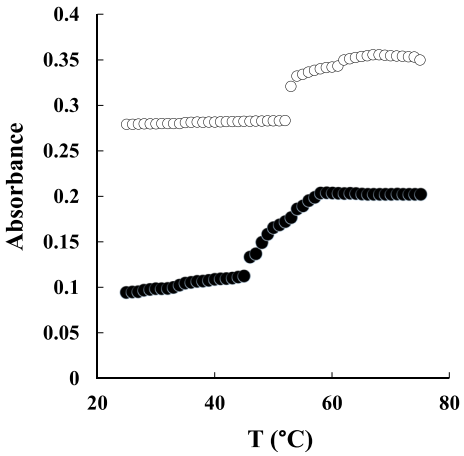

Fig. 10 Melting curve of HSA in the absence (●) and the presence of *cis*-[Pt $(NH_3)_2$(tertpentylgly)]NO_3 (○) in Tris-HCl buffer at 25 to 84 °C

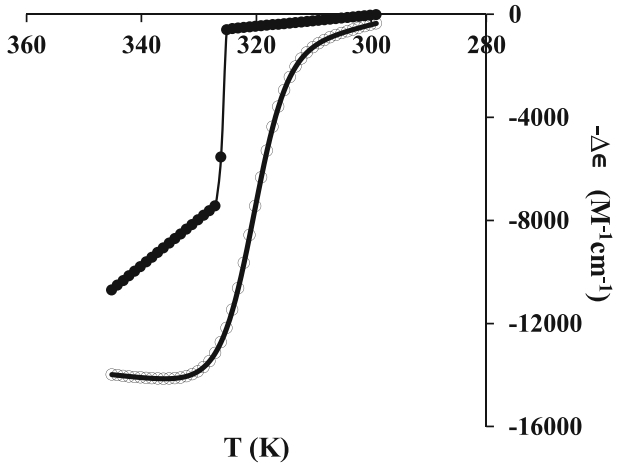

Fig. 11 Predicted changes absorption in **λ** = 278 nm vs. temperature using SigmaPlot software in the absence (○) and the presence (●) of Pt complex

$$A_0 = \frac{(A_N + KA_D)}{(1+K)} \tag{12}$$

On the other hand, the equilibrium constant can be determined by Eq. 13, where R is the gas constant and T is the study temperature.

$$K = \exp\left(\frac{-\Delta G^0}{RT}\right) \tag{13}$$

By substituting the k value in Eq. 12, Eq. 14 is gotten, and also in continuation by substituting the $\Delta G_D(T)$ in Eq. 14, Eq. 16 is obtained.

$$A_0 = \left[\frac{A_N + A_D e^{\left(\frac{-\Delta G^0}{RT}\right)}}{1 + e^{\left(\frac{-\Delta G^0}{RT}\right)}}\right] \tag{14}$$

$$A = \frac{A_N + A_D \exp\left[\frac{-\Delta H}{R}\left(\frac{1}{T} - \frac{1}{T_m}\right) - \Delta C_p\left[\frac{T_m}{T} - 1 + \ln\left(\frac{T}{T_m}\right)\right]\right]}{1 + \exp\left[\frac{-\Delta H}{R}\left(\frac{1}{T} - \frac{1}{T_m}\right) - \Delta C_p\left[\frac{T_m}{T} - 1 + \ln\left(\frac{T}{T_m}\right)\right]\right]} \tag{15}$$

Table 3 Fitted thermodynamic parameters of thermal denaturation of HSA and HSA-Pt complex

Fitting parameters	$a_N \times 10^{-3}$ (M^{-1} cm^{-1})	m_N (M^{-1} cm^{-1} K^{-1})	$a_D \times 10^{-3}$ (M^{-1} cm^{-1})	m_D (M^{-1} cm^{-1} K^{-1})	T_m (K)	ΔH_m (kJ/mol)
HSA	1.61	− 54.74	− 22.94	25.86	321.71	292
HSA-Pt complex	6.42	− 21.48	5.19	− 180	326.99	6268

Since $A_N = a_N + m_N T$ and $A_D = a_D + m_D T$ are linear functions at temperature, and also $\Delta\varepsilon_{280}$ is an adsorption coefficient change in any temperature (298 K) in $\lambda_{max} = 278$ nm for HSA in the absence and presence of Pt complex, Eq. 16 can be written as follows:

$$-\Delta\varepsilon_{280} = \frac{\Delta\varepsilon_N + \Delta\varepsilon_D \exp\left[\frac{-\Delta H}{R}\left(\frac{1}{T}-\frac{1}{T_m}\right)-\Delta C_p\left[\frac{T_m}{T}-1+\ln\left(\frac{T}{T_m}\right)\right]\right]}{1+\exp\left[\frac{-\Delta H}{R}\left(\frac{1}{T}-\frac{1}{T_m}\right)-\Delta C_p\left[\frac{T_m}{T}-1+\ln\left(\frac{T}{T_m}\right)\right]\right]} \quad (16)$$

All parameters in Eq. 16 can be determined by fitting and using SigmaPlot software. By using summarized data in Table 3, $\Delta G_D(T)$ at 25 to 75 °C by Eq. 10 can be calculated. The result is represented in Figs. 11 and 12. The result shows more stable state about $T_s = 319.15$ to 327.15 K.

Kinetic Study

Kinetic studies prepare the information about the possible mechanism of HSA interaction with Pt complex by the time scanning that recorded 1 min at 278 nm until 1 h [42].

The rate of HSA interaction with complex can be calculated by using Eqs. 17 and 18.

$$\frac{1}{A_\infty - A} = \frac{ak_2 t}{A_\infty - A} + \frac{1}{A_\infty - A_0} \quad (17)$$

$$\ln(A_\infty - A) = -ak_1 t + \ln(A_\infty - A_0) \quad (18)$$

Plots of $\ln(A_\infty - A)$ vs. time (s) and $\frac{1}{A_\infty - A}$ vs. time (s) time at 27 and 37 °C show that the kinetics is a quadratic reaction (Fig. 13).

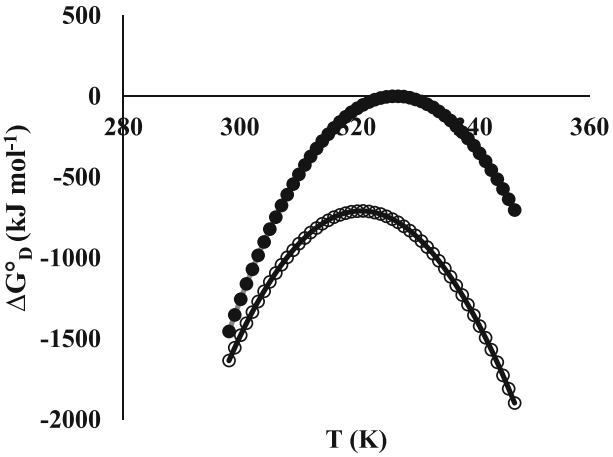

Fig. 12 HSA denaturation Gibbs free energy changes vs. temperature in the absence (○) and the presence (●) of Pt complex

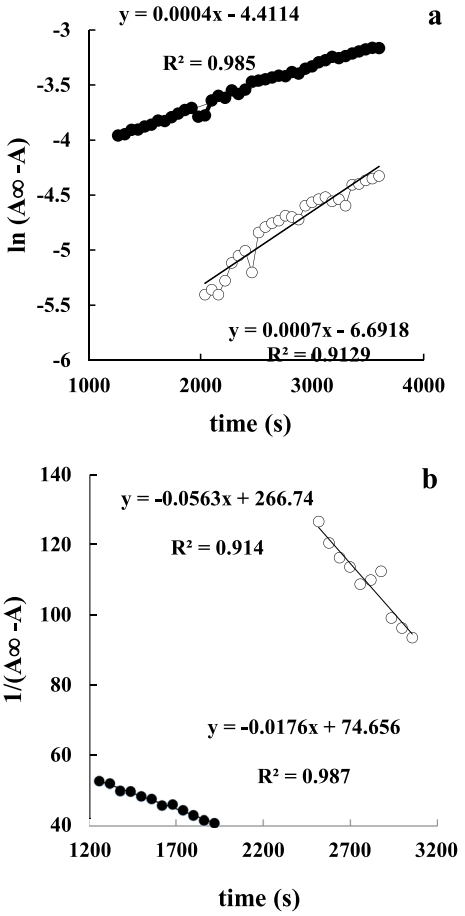

Fig. 13 Plot of $\ln(A_\infty - A)$ (**a**) and $\frac{1}{A_\infty - A}$ (**b**) vs. time (s) for HSA-complex interaction at 27 and 37 °C

Also, the diagram of absorption vs. time (Fig. 14) at 27 and 37 °C shown at first time scanning absorption is high and then it is fixed because the incubation process is completed at 27 °C. Increasing absorption is continued to 1500 s at 37 °C.

Fluorescence Titration Studies

Figure 15 displays the fluorescence quenching of HSA (7.5 μM) in the presence of different amounts of the *cis*-[Pt $(NH_3)_2$(tertpentylgly)]NO_3 (0 to 210 μM). Figure 15 shows by Pt (II) complex addition to HSA solution, reducing emission of fluorescence spectra was seen due to the primary interaction between synthesized Pt (II) complex and HSA. The mechanism (static or dynamic) of fluorescence quenching was determined by using the Stern-Volmer equation (Eqs. 19 and 20) [43], and F_0/F against [complex] was drowning at 298 K in the inset of Fig. 15.

$$\frac{F_0}{F} = 1 + K_{SV}[\text{complex}] \tag{19}$$

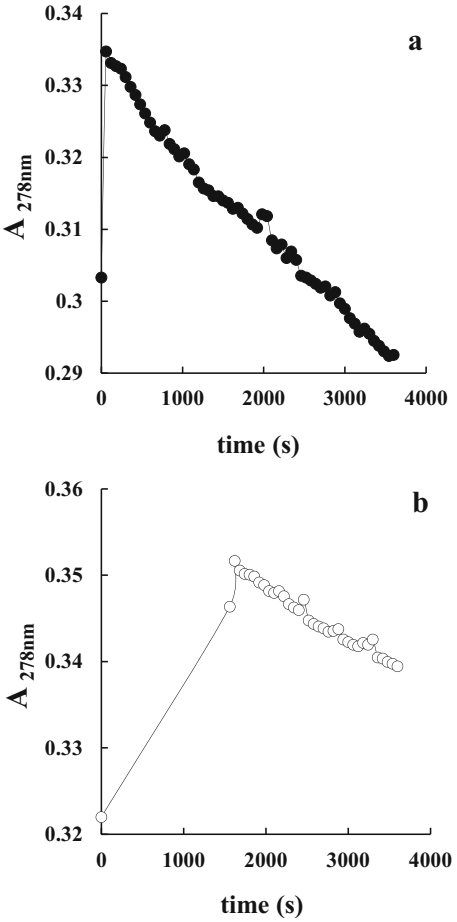

Fig. 14 Time scanning of HSA solution in the presence of complex at ri: $\frac{[\text{complex}]}{[\text{HSA}]} = 12.4$ at 27 °C (**a**) and 37 °C (**b**)

$$K_{SV} = k_q \tau_0 \tag{20}$$

Here, the fluorescence intensities of protein without and with quencher are F_0 and F, respectively, and also [complex] is quencher concentration, and K_{SV} is the Stern-Volmer quenching constant; k_q is the quenching velocity constant of HSA; τ_0 is the average lifetime of the HSA lacking any quencher and the fluorescence lifetime of the biopolymer is 10^{-8} s [43]. The linearity of this diagram offers a single type of quenching process [5]. Giving k_q from the rank 10^{11} M^{-1} s^{-1}, which is higher than maximal dynamic quenching constant($2 \times 10^{10} M^{-1} S^{-1}$). This means that by complex formation of a complex with static quenching is dominant in HSA-Pt complex [5].

Also, the binding constant (K_b) and the binding stoichiometry (g) for Pt complex-HSA formation were measured using Eq. 21.

$$\log\left(\frac{F_0 - F}{F}\right) = \log K_b + g\log[\text{complex}] \tag{21}$$

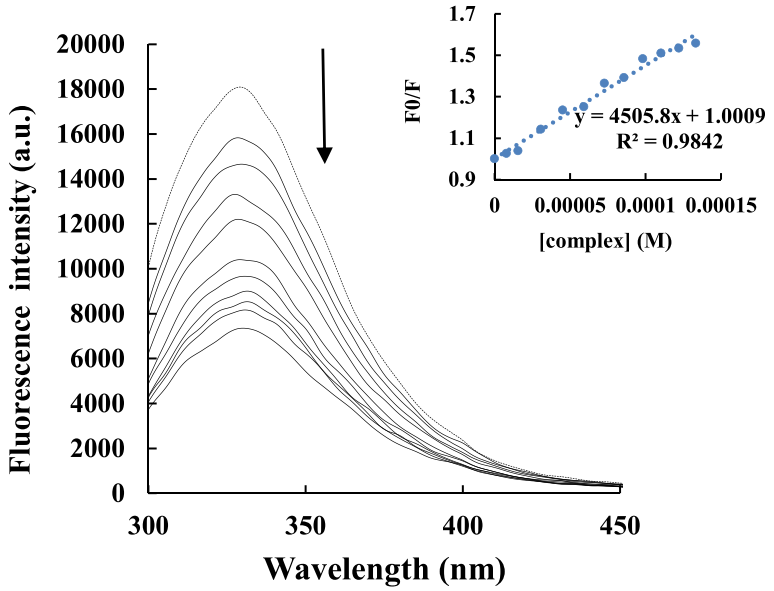

Fig. 15 The quenching intensity of HSA ($\lambda_{ex} = 280$ nm), in the presence (0 to 210 μM) of complex. In the inset: the Stern-Volmer plot of HSA quenching by metal complex

Binding data is summarized in Table 4. The K_b and g can be computed by the intercept and the slope of the double logarithm regression $\log(F_0 - F)/F$ vs. log [complex] [44]. According to the values of binding constant (K_b), as shown in Table 4, the platinum complex interacts with HSA moderately with values of around 10^4 M^{-1}.

The number of the binding site on HSA, g, is about one (Table 2), which indicates complex binds to HSA with the molar ratio of 1:1. In fact, binding complex on carrier protein and release it throughout the body should be done with suitable affinity. Also, to release a drug in its target, K_b should not be very high. The obtained HSA-binding constant of complex is in a good range ($1 - 6 \times 10^4 M^{-1}$) [36].

The average aggregation number of HSA, <*J*>, potentially induced by complex can be determined by quenching data analysis [45]. It is shown in Eq. 22.

$$1 - \frac{F}{F_0} = \langle J \rangle \frac{[\text{complex}]}{[\text{HSA}]_0} \tag{22}$$

Figure 16 shows the changes of $1 - \frac{F}{F_0}$ vs. $\frac{[\text{complex}]}{[\text{HSA}]_0}$molar ratio.

The <*J*> values, obtained by the slope of the lines in Fig. 16, that are listed in Table 3 indicate that *cis*-[Pt $(NH_3)_2$(tertpentylgly)]NO_3 binding does not induce any aggregation in HSA molecules and consequently confirm the 1:1 stoichiometry for complex-HSA complex [45].

Table 4 The quenching and binding data of HSA-complex formation

Complex	$K_{SV}(M)^{-1}$	$k_q(MS)^{-1}$	R^2	$K_b(M)^{-1}$	n	R^2	$\langle J \rangle$	R^2
cis-[Pt $(NH_3)_2$(tertpentylgly)]NO_3	4.50×10^3	4.50×10^{11}	0.98	3.99×10^4	1.22	0.98	0.01	0.98

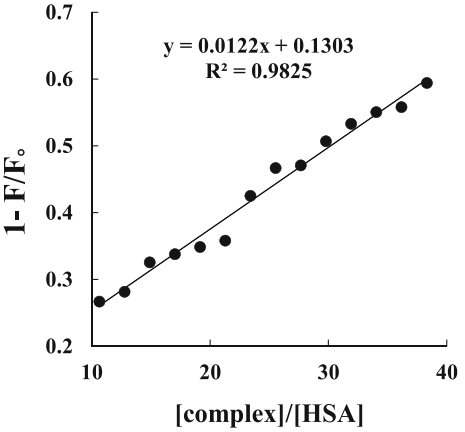

Fig. 16 Determination of the average aggregation number of HSA (<*J*>) in the presence of *cis*-[Pt $(NH_3)_2$(tertpentylgly)]NO_3. . λ_{ex} = 280 nm, λ_{em} = 590 nm, and spectral bandwidth is 5 nm for both excitation and emission slits

Cyclic Voltammetry Results

For understanding the HSA-binding modes, the cyclic voltammogram of the complex in the absence and presence of HSA is recorded and shown in Fig. 17. Complex showed one anodic peak at − 0.366 V with corresponding peak current 2.475×10^{-5} μA in Tris buffer of pH 7.4– and cathodic peak at − 0.923 V with 3.757×10^{-5} μA. Also, in the presence of HSA, the anodic peak potential was shown at − 0.528 V with corresponding peak current 5.41×10^{-5} μA cathodic peak at − 0.894 V with corresponding peak current 4.64×10^{-5} μA. This negative shift at anodic peak was considered as evidence for the binding of complex on HSA via electrostatic interaction [42].

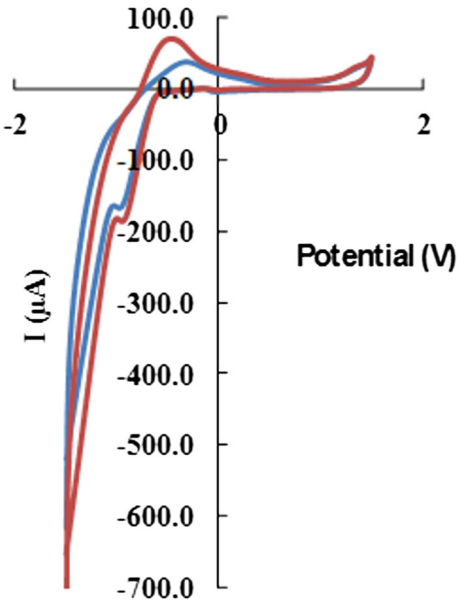

Fig. 17 Cyclic voltammogram of [Pt $(NH_3)_2$(tertpentylgly)]NO_3 complex (0.1 mM) in the absence (blue) and presence of HSA (red) in 10 mM Tris-HCl, pH 7.4

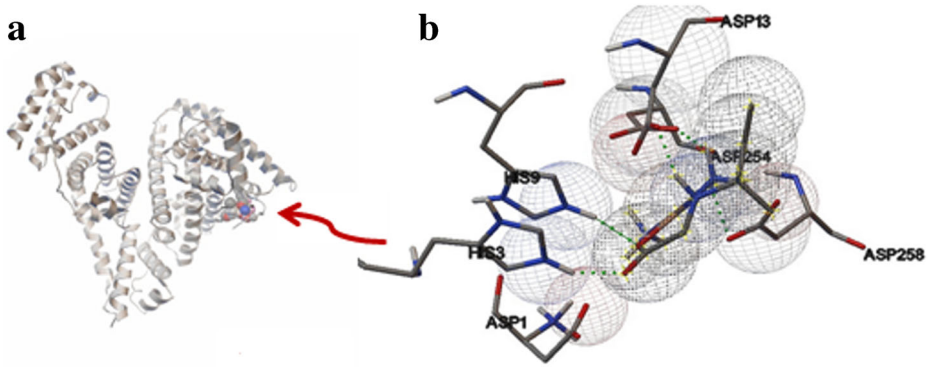

Fig. 18 **a** Docking site of the most negative cluster in the complex-HSA system. **b** Amino acid residues surrounding Pt complex

Molecular Docking

For calculating the grids, AutoGrid was used by adding the Gasteiger charges to provide the 5ORI input file for docking.

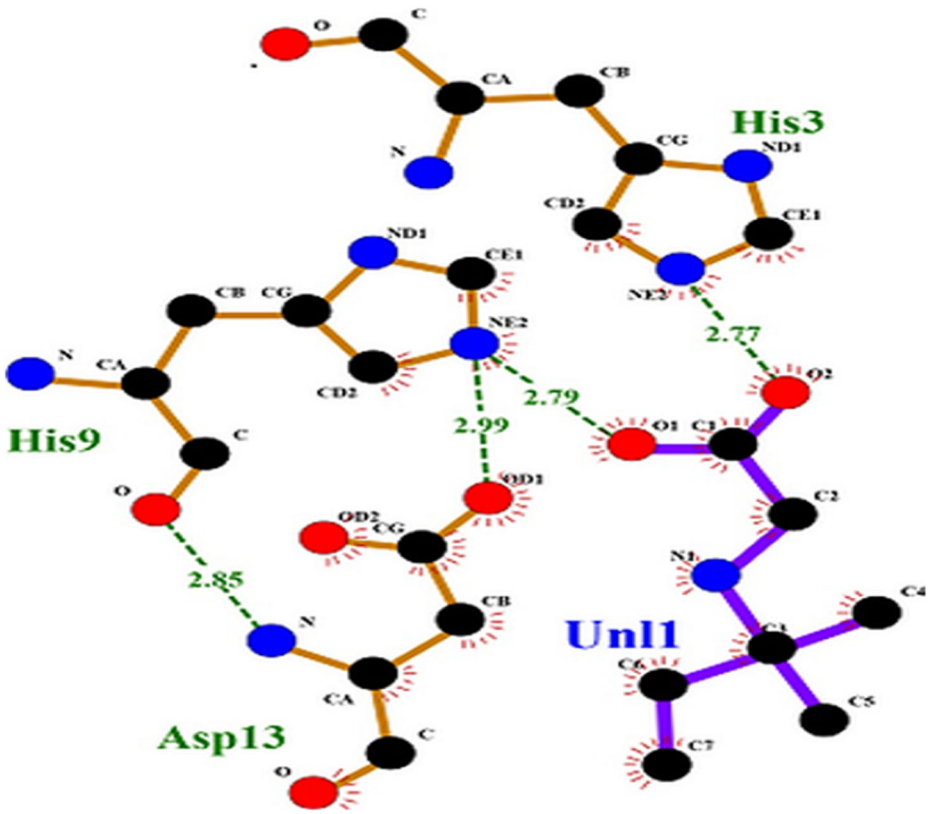

Fig. 19 Two-dimensional interactions between complex and HSA generated by LIGPLOT

Docking building with 126 lattice points along the axes *X*, *Y*, and *Z* was done to determine the active site of the Pt complex on HSA. After designation of the active site, the dimensions of the grid map were chosen as 80 points on a side with a grid point spacing of 0.375 Å, to allow the complex to rotate freely. One hundred docking runs with 25,000,000 energy valuation for each run were performed [46, 47]. The value of the binding energy for complex-HSA formation is − 16.2 kcal mol^{-1}, and also complex binds with hydrogen interaction in the site I subdomain IIA of HSA (Asp13, Asp254, Asp258, His3, His9). Figures 18 and 19 show molecular docking analysis by AutoDock Tools and LIGPLOT. Both figures show binding site and analysis of the molecular docking.

Conclusions

In the present article, the synthesis and characterization of complex were accomplished. This water-soluble compound was evaluated for its anticancer activity against human breast cancer cell line. IC_{50} value of Pt complex in MCF-7 cell line was calculated 175 μL, which is higher than that of the cisplatin with $IC_{50} = 80$ μM. Then, binding of HSA with a complex was studied under simulated physiological conditions by using the fluorescence, UV-Vis, cyclic voltammetry, and molecular docking methods. According to the results from different spectroscopic methods, *cis*-[Pt $(NH_3)_2$(tertpentylgly)]NO_3 binds to HSA with high affinity through a static mode because k_q is more than 2×10^{10} M^{-1} s^{-1}. The standard Gibbs free energy of binding of Pt complex to HSA was negative, and then this interaction was spontaneous. The negative ΔH_b° and positive ΔS_b° indicate electrostatic interactions are the main role during the complex binding on HSA as CV result indicates this interaction too. The molecular docking study indicates complex binds to the site I subdomain IIA of HSA.

Acknowledgments The authors of this article would like to thank Payame Noor University of Isfahan.

References

1. Yang, F., Zhang, Y., & Liang, H. (2014). Interactive association of drugs binding to human serum albumin. *International Journal of Molecular Sciences, 15*, 3580–3595. https://doi.org/10.4172/2254-609X.100033.
2. Yasseen, Z. J., & El-Ghossain, M. O. (2016). Studies on binding of widely used drugs with human serum albumin at different temperatures and PHs. *Journal of Biomedical Science, 5*, 19–27. https://doi.org/10.4172/2254-609X.100033.
3. Tan, X., & Song, Z. (2014). Relationship investigation of molecular structure–binding affinity of antibiotics to bovine serum albumin using flow injection chemiluminescence analysis and molecular docking. *RSC Advances, 4*, 3263–3271. https://doi.org/10.1039/c3ra45885g.
4. Shahabadi, N., & Nemati, L. (2014). Multispectroscopic studies on the interaction of a platinum (II) complex containing l-histidine and 1, 10-phenanthroline ligands with bovine serum albumin. *Applied Biochemistry and Biotechnology, 172*, 2800–2814. https://doi.org/10.1007/s12010-013-0715-z.
5. Divsalar, A., Zhila, I., Saboury, A. A., Nabiuni, M., Razmi, M., & Mansuri-Torshizi, H. (2013). Cytotoxic and spectroscopic studies on binding of a new synthesized bipyridine ethyl dithiocarbamate Pt (II) nitrate complex to the milk carrier protein of BLG. *Journal of the Iranian Chemical Society, 10*, 951–959. https://doi.org/10.1007/s13738-013-0232-6.
6. Ndagi, U., Mhlongo, N., & Soliman, M. E. (2017). Metal complexes in cancer therapy–an update from drug design perspective. *Drug Design, Development and Therapy, 11*, 599–616. https://doi.org/10.2147/DDDT.S119488.

7. Chuang, V. T. G., Maruyama, T., & Otagiri, M. (2009). Updates on contemporary protein binding techniques. *Drug Metabolism and Pharmacokinetics, 24*, 358–364. https://doi.org/10.2133/dmpk.24.358.
8. Summa, N., Schiessl, W., Puchta, R., van Eikema Hommes, N., & van Eldik, R. (2006). Thermodynamic and kinetic studies on reactions of Pt (II) complexes with biologically relevant nucleophiles. *Inorganic Chemistry, 45*, 2948–2959. https://doi.org/10.1021/ic051955r.
9. Yousefi, R., Aghevlian, S., Mokhtari, F., Samouei, H., Rashidi, M., Nabavizadeh, S. M., Tavaf, Z., Pouryasin, Z., Niazi, A., Faghihi, R., & Papari, M. M. (2012). The anticancer activity and HSA binding properties of the structurally related platinum (II) complexes. *Applied Biochemistry and Biotechnology, 167*, 861–872. https://doi.org/10.1007/s12010-012-9733-5.
10. Zheng, Y. R., Suntharalingam, K., Johnstone, T. C., Yoo, H., Lin, W., Brooks, J. G., & Lippard, S. J. (2014). Pt (IV) prodrugs designed to bind non-covalently to human serum albumin for drug delivery. *Journal of the American Chemical Society, 136*, 8790–8798. https://doi.org/10.1021/ja50382.
11. Saeidifar, M., & Mansouri-Torshizi, H. (2015). Investigation of the interaction between human serum albumin and antitumor palladium (II) complex containing 1, 10-phenanthroline and dithiocarbamate ligands. *Nucleosides, Nucleotides & Nucleic Acids, 34*, 16–32. https://doi.org/10.1080/15257770.2014.955192.
12. Lin, X. D., Liu, Y. H., Xie, C. Z., Bao, W. G., Shen, J., & Xu, J. Y. (2017). Three Pt (II) complexes based on thiosemicarbazone: synthesis, HSA interaction, cytotoxicity, apoptosis and cell cycle arrest. *RSC Advances, 7*, 26478–26486. https://doi.org/10.1039/c7ra04443.
13. Shahabadi, N., & Hadidi, S. (2015). Mechanistic and conformational studies on the interaction of a platinum (II) complex containing an antiepileptic drug, levetiracetam, with bovine serum albumin by optical spectroscopic techniques in aqueous solution. *Applied Biochemistry and Biotechnology, 175*, 1843–1857. https://doi.org/10.1007/s12010-014-1423-z.
14. Coban, B., & Yildia, U. (2014). DNA-binding studies and antitumor evaluation of novel water soluble organic pip and hpip analogs. *Applied Biochemistry and Biotechnology, 172*, 248–262. https://doi.org/10.1007/s12010-013-0513-7.
15. Dehkhodaei, M., Sahihi, M., Rudbari, H. A., Ariaeefar, M., Gharaghani, S., Azadbakht, R., Taheri, S., & Kajani, A. A. (2018). Multi experimental and computational studies for DNA and HSA interaction of new nano-scale ultrasound-assisted synthesized Pd (II) complex as a potent anticancer drug. *Journal of Molecular Liquids, 264*, 386–397. https://doi.org/10.1016/j.molliq.2018.05.077.
16. Chandrasekhar, V. R., Mookkandi Palsamy, K., Lokesh, R., Jegathalaprathaban, R., & Gurusamy, R. (2019). Biomolecular docking, antimicrobial and cytotoxic studies on new bidentate schiff base ligand derived metal (II) complexes. *Applied Organometallic Chemistry, 33*, e4753. https://doi.org/10.1002/a0c.4753.
17. Dhahagani, K., Kesavan, M. P., Vinoth, K. G. G., Ravi, L., Rajagopal, G., & Rajesh, J. (2018). Crystal structure, optical properties, DFT analysis of new morpholine based Schiff base ligands and their copper (II) complexes: DNA, protein docking analyses, antibacterial study and anticancer evaluation. *Materials Science and Engineering: C, 90*, 119–130. https://doi.org/10.1016/j.msec.2018.034.032.
18. Gubendran, A., Kesavan, M. P., Ayyanaar, S., Raja, J. D., Athappan, P., & Rajesh, J. (2017). Synthesis and characterization of water-soluble copper (II), cobalt (II) and zinc (II) complexes derived from 8-hydroxyquinoline-5-sulphonic acid: DNA binding and cleavage studies. *Applied Organometallic Chemistry, 31*, e3708. https://doi.org/10.1002/aoc.3708.
19. Gubendran, A., Kesavan, M. P., Ayyanaar, S., Mitu, L., Athappan, P., & Rajesh, J. (2017). Non-enolisable Knoevenagel condensate appended Schiff bases-metal (II) complexes: spectral characteristics, DNA-binding and nuclease activities. *Spectrochimica Acta A, 181*, 39–46. https://doi.org/10.1016/j.saa.2017.03.031.
20. Kesavan, M. P., Kumar, G. G. V., Anitha, K., Ravi, L., Raja, J. D., Rajagopal, G., & Rajesh, J. (2017). Natural alkaloid luotonin A and its affixed acceptor molecules: serum albumin binding studies. *Journal of Photochemistry and Photobiology B, 173*, 499–507. https://doi.org/10.1016/j.jphotobiol.2017.06.030.
21. Kantoury, M., Eslami Moghadam, M., Tarlani, A. A., & Divsalar, A. (2016). Structure effect of some new anticancer Pt (II) complexes of amino acid derivatives with small branched or linear hydrocarbon chains on their DNA interaction. *Chemical Biology & Drug Design, 88*, 76–87. https://doi.org/10.1111/cbdd.12735.
22. Abyaneh, F. S. S., Moghadam, M. E., Divsalar, A., Ajloo, D., & Sadr, M. H. (2018). Improving of anticancer activity and solubility of cisplatin by methylglycine and methyl amine ligands against human breast adenocarcinoma cell line. *Applied Biochemistry and Biotechnology, 186*, 271–291. https://doi.org/10.1007/s12010-018-2715-5.
23. Hadian Rasanani, S., Eslami Moghadam, M., Soleimani, E., Divsalar, A., & Tarlani, A. (2017). Improving activity of anticancer oxalipalladium analog by the modification of oxalate group with isopentylglycine. *Journal of Coordination Chemistry, 70*, 3769–3789. https://doi.org/10.1080/00958972.2017.1395417.
24. Kandagal, P. B., Ashoka, S., Seetharamappa, J., Vani, V., & Shaikh, S. M. T. (2006). Study of the interaction between doxepin and human serum albumin by spectroscopic methods. *Journal of Photochemistry and Photobiology A, 179*, 161–166. https://doi.org/10.1016/j.jphotochem.2005.08.008.

25. Dehkhodaei, M., Sahihi, M., Rudbari, H. A., & Momenbeik, F. (2018). DNA and HSA interaction of vanadium (IV), copper (II), and zinc (II) complexes derived from an asymmetric bidentate Schiff-base ligand: multi spectroscopic, viscosity measurements, molecular docking, and ONIOM studies. *Journal of Biological Inorganic Chemistry, 23*, 181–192. https://doi.org/10.1007/s00775-017-1505-9.
26. Khosravi, I., Sahihi, M., Rudbari, H. A., Borhan, G., & Chavoshpour-Natanzi, Z. (2017). The interaction of a new Schiff base ligand with human serum albumin: molecular docking and molecular dynamics simulation studies. *Journal of Macromolecular Science Part B, 56*, 636–643. https://doi.org/10.1080/00222348.2017.1356634.
27. Eslami Moghadam, M., Divsalar, A., Abolhosseini Shahrnoy, A., & Saboury, A. A. (2016). Synthesis, cytotoxicity assessment, and interaction and docking of novel palladium (II) complexes of imidazole derivatives with human serum albumin. *Journal of Biomolecular Structure & Dynamics, 34*, 1751–1762. https://doi.org/10.1080/07391102.2015.1090345.
28. Bi, S., Song, D., Tian, Y., Zhou, X., Liu, Z., & Zhang, H. (2005). Molecular spectroscopic study on the interaction of tetracyclines with serum albumins. *Spectrochimica Acta A, 61*, 629–636. https://doi.org/10.1016/j.saa.2004.05.028.
29. Xu, L., Hu, Y. X., Li, Y. C., Liu, Y. F., Zhang, L., Ai, H. X., & Liu, H. S. (2017). Study on the interaction of paeoniflorin with human serum albumin (HSA) by spectroscopic and molecular docking techniques. *Chemistry Central Journal, 11*, 116–128. https://doi.org/10.1186/s13065-017-0348-3.
30. Heydari, M., Moghadam, M. E., Tarlani, A., & Farhangian, H. (2017). DNA as a target for anticancer phen-imidazole Pd (II) complexes. *Applied Biochemistry and Biotechnology, 182*, 110–127. https://doi.org/10.1007/s12010-016-2314-2.
31. Stephanos, J. J. (1996). Drug-protein interactions: two-site binding of heterocyclic ligands to a monomeric hemoglobin. *Journal of Inorganic Biochemistry, 62*, 155–169. https://doi.org/10.1016/0162-0134(95)00144-1.
32. Aghaee, E., Ghasemi, J. B., Manouchehri, F., & Balalaie, S. (2014). Combined docking, molecular dynamics simulations and spectroscopic studies for the rational design of a dipeptide ligand for affinity chromatography separation of human serum albumin. *Journal of Molecular Modeling, 20*, 2446–2459. https://doi.org/10.1007/s00894-014-2446-7.
33. Fu, X. B., Liu, D. D., Lin, Y., Hu, W., Mao, Z. W., & Le, X. Y. (2014). Water-soluble DNA minor groove binders as potential chemotherapeutic agents: synthesis, characterization, DNA binding and cleavage, antioxidation, cytotoxicity and HSA interactions. *Dalton Transactions, 43*, 8721–8737. https://doi.org/10.1039/c3dt53577k.
34. Bordbar, A. K., Saadati, Z., & Sohrabi, N. (2004). Analysis of ligand binding process using binding capacity concept. *Acta Biochimica Polonica, 51*, 963–970.
35. Ascenzi, P., Bocedi, A., Notari, S., Fanali, G., Fesce, R., & Fasano, M. (2006). Allosteric modulation of drug binding to human serum albumin. *Medicinal Chemistry, 6*, 483–489. https://doi.org/10.2174/138955706776361448.
36. Ajloo, D., Moghadam, M. E., Ghadimi, K., Ghadamgahi, M., Saboury, A. A., Divsalar, A., Sheikhmohammadi, M., & Yousefi, K. (2015). Synthesis, characterization, spectroscopy, cytotoxic activity and molecular dynamic study on the interaction of three palladium complexes of phenanthroline and glycine derivatives with calf thymus DNA. *Inorganica Chimica Acta, 430*, 144–160. https://doi.org/10.1016/j.ica.2015.03.006.
37. Rippe, K. (1997). Analysis of protein-DNA binding at equilibrium. *B. I. F Futura, 12*, 20–26.
38. Bordbar, A. K., Sohrabi, N., & Hojjati, E. (2004). The estimation of the hydrophobic and electrostatic contributions to the free energy change upon cationic surfactants binding to Jack bean urease. *Colloids and Surfaces. B, Biointerfaces, 39*, 171–175. https://doi.org/10.1016/j.colsurfb.2004.07.009.
39. Liu, P., Liu, J., Zhang, Y. Q., Wu, B. Y., & Wang, K. Z. (2015). Synthesis, DNA binding and photocleavage, and cellular uptake of an alkyl chain-linked dinuclear ruthenium (II) complex. *Journal of Photochemistry and Photobiology. B, 143*, 89–99. https://doi.org/10.1016/j.jphotobiol.2015.01.004.
40. Sohrabi, N., Rasouli, N., & Raissi, M. (2017). Study the interaction of Ni complex of tetradentate schiff base ligand with hen egg white lysozyme. *Physical and Chemical Research, 5*, 113–123. https://doi.org/10.22036/pcr.2017.38593.
41. Hadian Rasanani, S., Eslami Moghadam, M., Soleimani, E., Divsalar, A., Ajloo, D., Tarlani, A., & Amiri, M. (2018). Anticancer activity of new imidazole derivative of 1R, 2R-diaminocyclohexane palladium and platinum complexes as DNA fluorescent probes. *Journal of Biomolecular Structure & Dynamics, 36*, 3058–3076. https://doi.org/10.1080/07391102.2017.1385538.
42. Varlan, A., Ionescu, S., & Hillebrand, M. (2011). Study of the interaction between ofloxacin and human serum albumin by spectroscopic methods. *Luminescence, 26*, 710–715. https://doi.org/10.1002/bio.1302.
43. Shahabadi, N., & Amiri, S. (2015). Spectroscopic and computational studies on the interaction of DNA with pregabalin drug. *Spectrochimica Acta A, 138*, 840–845. https://doi.org/10.1016/j.saa.2014.10.104.

44. Bordbar, A. K., Dezhampanah, H., Asadi, M., Safaei, E., Sohrabi, N., & Khodadost, Y. (2007). Thermodynamics investigation of a series of metalloporphyrazine-bovine serum albumin complexes. *Journal of Porphyrins and Phthalocyanines, 11*, 556–565. https://doi.org/10.1142/S1088424607000655.
45. Anjomshoa, M., Torkzadeh-Mahani, M., Sahihi, M., Rizzoli, C., Ansari, M., Janczak, J., Sherafat Esfahani, S., Ataei, F., Dehkhodaei, M., & Amirheidari, B. (2018). Tris-chelated complexes of nickel (II) with bipyridine derivatives: DNA binding and cleavage, BSA binding, molecular docking, and cytotoxicity. *Journal of Biomolecular Structure & Dynamics, 11*, 1–51. https://doi.org/10.1080/07391102.2018.1534700.
46. Ghosh, P., Devi, G. P., Priya, R., Amrita, A., Sivaramakrishna, A., Babu, S., & Siva, R. (2013). Spectroscopic and in silico evaluation of interaction of DNA with six derivatives. *Applied Biochemistry and Biotechnology, 170*, 1127–1137. https://doi.org/10.1007/s12010-013-0259-2.
47. Hosseinzadeh, R., Bordbar, A. K., Matin, A. A., & Maleki, R. (2007). Potentiometric study of cetylpyridinium chloride cooperative binding to anionic azo-dyes. *Journal of the Brazilian Chemical Society, 18*, 359–363. https://doi.org/10.1590/S0103-50532007000200017.

Affiliations

Afrooz Shiekhzadeh[1] · Nasrin Sohrabi[1] · Mahboube Eslami Moghadam[2] · Mohsen Oftadeh[1]

[1] Department of Chemistry, Payame Noor University (PNU), Tehran, Iran

[2] Chemistry & Chemical Engineering Research Center of Iran, Tehran, Iran